Available online at www.sciencedirect.com
SCIENCE DIRECT®
ELSEVIER
Nuclear Physics A 761 (2005) 162–172
NUCLEAR PHYSICS A

The ^{8}Li$(d, p)^{9}$Li reaction and astrophysical ^{8}B$(p, \gamma)^{9}$C reaction rate

B. Guo, Z.H. Li *, W.P. Liu, X.X. Bai, G. Lian, S.Q. Yan, B.X. Wang, S. Zeng, J. Su, Y. Lu

China Institute of Atomic Energy, P.O. Box 275(46), Beijing 102413, PR China

Received 15 April 2005; received in revised form 16 June 2005; accepted 6 July 2005

Available online 8 August 2005

Abstract

Angular distribution of the ^{8}Li$(d, p)^{9}$Li$_{g.s.}$ reaction at $E_{cm} = 7.8$ MeV was measured in inverse kinematics. The square of asymptotic normalization coefficient (ANC) for the virtual decay $^{9}\text{Li} \rightarrow {}^{8}\text{Li} + n$ was derived to be 1.33 ± 0.33 fm^{-1} through distorted wave Born approximation (DWBA) analysis, for the first time. According to charge symmetry, (ANC)^2 for $^{9}\text{C} \rightarrow {}^{8}\text{B} + p$ was then extracted to be 1.14 ± 0.29 fm^{-1}. We have deduced the astrophysical S-factors and reaction rates for direct capture in ^{8}B$(p, \gamma)^{9}$C at energies of astrophysical relevance using the ANC for $^{9}\text{C} \rightarrow {}^{8}\text{B} + p$ extracted from the mirror system.

PACS: 25.60.Je; 21.10.Jx; 25.40.Lw; 26.20.+f

Keywords: NUCLEAR REACTIONS ^{2}H(^{8}Li, ^{9}Li), $E_{cm} = 7.8$ MeV; measured $\sigma(\theta)$, DWBA analysis; deduced asymptotic normalization coefficient; mirror systems; ^{8}B(p, γ), $E =$ low; deduced astrophysical S-factor

1. Introduction

Nucleosynthesis of light nuclei is impeded by the gap at mass number $A = 8$, where no stable nuclei exist. In some astrophysical environments, however, this gap

* Corresponding author.
E-mail address: zhli@iris.ciae.ac.cn (Z.H. Li).

0375-9474/$ – see front matter
doi:10.1016/j.nuclphysa.2005.07.013

can be bypassed via the reactions involving unstable nuclei ^{8}B and ^{8}Li, such as ^{8}B$(p,\gamma)^9$C, ^{8}Li$(\alpha,n)^{11}$B, ^{8}Li$(n,\gamma)^9$Li and ^{8}Li$(d,p)^9$Li, to synthesize $A > 8$ nuclides. The ^{7}Be$(p,\gamma)^8$B$(p,\gamma)^9$C$(\alpha,p)^{12}$N$(p,\gamma)^{13}$O reaction chain is considered as one of the possible alternative paths to the 3α process for transforming the nuclei in the pp chains to the CNO nuclei in the peculiar astrophysical sites where the densities ($\geqslant 2 \times 10^7$ g/cm^3) and temperatures ($T_9 \sim 0.1$–0.4) are so high that the proton- and α-capture reactions become faster than the competing β-decays [1]. The ^{8}B$(p,\gamma)^9$C reaction may play an important role in the evolution of massive stars with very low metallicities [1,2], and thus has increasingly attracted both theoretical and experimental studies [1,3–8]. There are several microscopic and systematic calculations, and their results are in large discrepancy [1,3,4]. As for the experiments, it is very difficult to directly measure this reaction at energies of astrophysical relevance because of very small cross section and low intensity of the available ^{8}B beam at present. Some indirect approaches have been applied to the study of this reaction [5–8]. Beaumel et al. [5] measured the ^{8}B$(d,n)^9$C angular distribution in inverse kinematics with a 14.4 A MeV ^{8}B beam, and then derived the ANC for the virtual decay $^9\mathrm{C} \rightarrow {}^8\mathrm{B} + p$ and the astrophysical $S_{18}(0)$ factor for the ^{8}B$(p,\gamma)^9$C reaction. Trache et al. [6] analyzed the cross section data for one-proton-removal reaction of ^{9}C on four different targets (C, Al, Sn and Pb) [9], and employed the Glauber model [10] to deduce the ANC and $S_{18}(0)$ factor. Recently, Motobayashi [7] extracted the S_{18} factors in energy range 0.2–0.6 MeV by Coulomb dissociation approach ($S_{18}(0)$ factor can be then obtained through an extrapolation by the slope of theoretical S-factor curve). Most recently, Enders et al. [8] studied the proton-removal from ^{9}C on a carbon target at $E = 78.3$ A MeV and derived the ANC and astrophysical $S_{18}(0)$ factor. The $S_{18}(0)$ obtained from Ref. [7] is significantly larger than other three ones.

The ^{8}Li$(d,p)^9$Li reaction not only leads to the production of ^{9}Be (via the ^{9}Li β-decay) which acts as a precursor to heavier nuclides, but also can serve as a surrogate reaction to extract the ^{8}B$(p,\gamma)^9$C and ^{8}Li$(n,\gamma)^9$Li reaction rates for the direct capture. To date, only a few experiments for the ^{8}Li$(d,p)^9$Li reaction have been carried out by using the secondary ^{8}Li beam. An earlier measurement, performed at $E_{\mathrm{cm}} = 1.5$–2.8 MeV [11], presented an upper limit of the cross section, though no ^{9}Li event was detected. Very recently, the angular distributions for different states in ^{9}Li were measured at $E(^8\mathrm{Li}) = 76$ MeV to obtain information on the spins, parities and single-neutron spectroscopic factors [12]. In the present work, we measured the ^{8}Li$(d,p)^9\mathrm{Li}_{\mathrm{g.s.}}$ angular distribution at $E(^8\mathrm{Li}) = 39$ MeV through the coincidence detection of ^{9}Li and recoil proton, and derived the ANC for the virtual decay $^9\mathrm{Li} \rightarrow {}^8\mathrm{Li} + n$ based on DWBA analysis, and then deduced the ANC for $^9\mathrm{C} \rightarrow {}^8\mathrm{B} + p$ based on charge symmetry. We have also calculated the direct capture S-factors and reaction rates for ^{8}B$(p,\gamma)^9$C at astrophysically relevant energies. Most recently, a short paper concerning the ^{8}Li$(d,p)^9\mathrm{Li}_{\mathrm{g.s.}}$ angular distribution and indirect determination of the astrophysical ^{8}Li$(n,\gamma)^9\mathrm{Li}_{\mathrm{g.s.}}$ reaction rates has been published elsewhere [13].

2. Experimental procedure and results

The measurement of ^{8}Li$(d,p)^9$Li angular distribution was performed using the secondary beam facility GIRAFFE [14,15] built at the HI-13 tandem accelerator of China

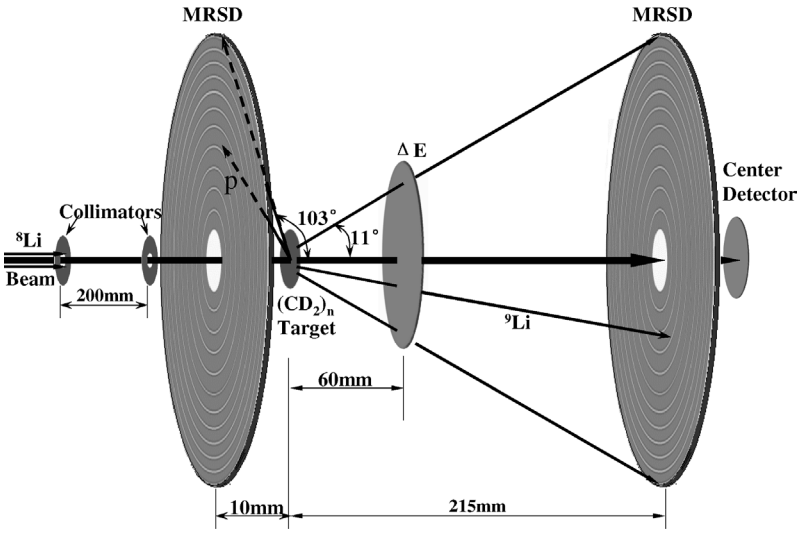

Fig. 1. Schematic layout of the experimental setup.

Institute of Atomic Energy. A 44 MeV ^{7}Li primary beam from the tandem accelerator impinged on a deuterium gas cell at 1.6 atm pressure to produce the ^{8}Li ions through the ^{2}H(^{7}Li, ^{8}Li)^{1}H reaction. The front and rear windows of the gas cell were 1.9 mg/cm^2 thick Havar foils. Following the magnetic separation and focus with a dipole and a quadrupole doublet, the 39 MeV secondary ^{8}Li beam was delivered. Typical purity of the ^{8}Li beam was about 80%, the main contaminants were ^{7}Li ions from Rutherford scattering of the primary beam in the gas cell windows and the beam tube.

The experimental setup is shown in Fig. 1. After the collimation using two $\varnothing$3 mm apertures, the ^{8}Li beam was directed onto a $(CD_2)_n$ target with a thickness of 1.5 mg/cm^2 to study the ^{2}H(^{8}Li, ^{9}Li)^{1}H reaction. A 1.8 mg/cm^2 thick carbon target served as the background measurement. The typical beam intensity on the target was approximately 1000 pps. The beam energy spread on the target was 0.52 MeV full width half maximum (FWHM) for long term measurement, and the beam angular divergence was about $\pm 0.3^\circ$. We utilized two 300 μm thick multi-ring semiconductor detectors (MRSDs) with center holes. The upstream MRSD was aimed at detection of the recoil protons, and the downstream one, backed by an independent 300 μm thick silicon detector placed at center hole, served as a residue energy (E_r) detector which formed a ΔE–E_r counter telescope together with a 21.7 μm thick silicon ΔE detector. Such a detector configuration covered the laboratory angular ranges of 0° to 11° (greater than the maximum θ_lab of ^{9}Li, 10.7°, thus enabled 100% detection of ^{9}Li ions due to the inverse kinematics), and 103° to 170° (for the recoil proton detection), respectively. For coincidence measurement, the detectable angular range of ^{9}Li in center of mass system was from 10° to 50°.

Recorded by the same counter telescope, the accumulated quantity of incident ^{8}Li ions for measurement with the $(CD_2)_n$ target was approximately 1.66×10^8, and 1.11×10^7 for that with the carbon target. Fig. 2(a) shows the coincidence ΔE–E_r scatter plot of the events detected by all rings of downstream MRSD with those detected by all rings of

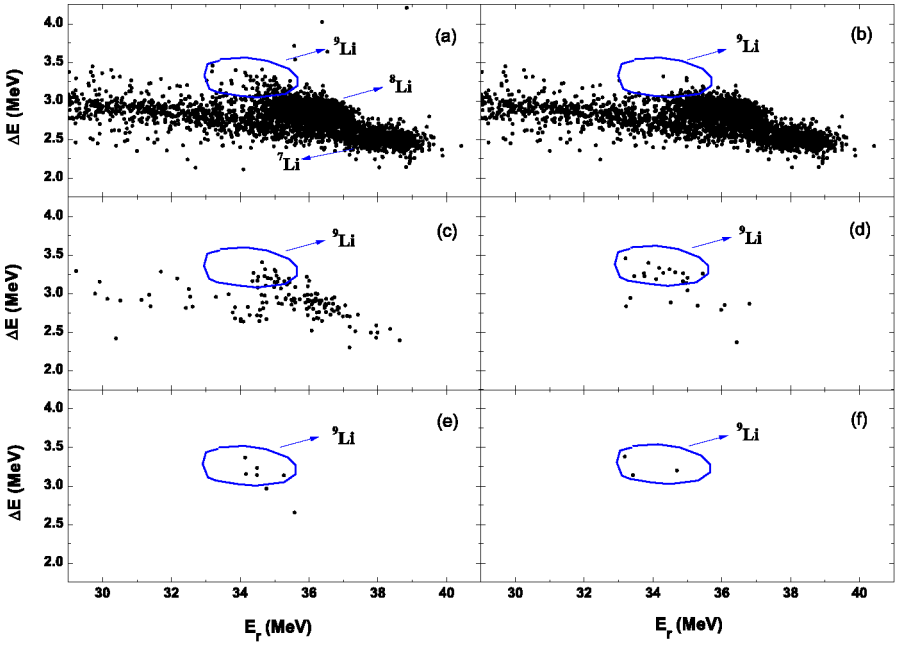

Fig. 2. Two-dimensional spectra of ΔE vs. $E_{\rm r}$ for the ^{9}Li-proton coincidence measurement with $(CD_2)_n$ target. (a) shows the coincidence ΔE–$E_{\rm r}$ spectrum of the events detected by all rings of downstream MRSD with those detected by all rings of upstream one. (b)–(f) display separately the coincidence ΔE–$E_{\rm r}$ spectra for the first to fifth rings of downstream MRSD.

upstream one. The events out of ^{9}Li region result from the random coincidence caused by the noise tail in the proton spectrum of the upstream MRSD. Actually, the selection of ^{9}Li events was individually performed for each ring of downstream MRSD. For the ^{9}Li events appearing on a specific ring of downstream MRSD, kinematics restricts the energies and angles of relevant protons detected by upstream one. Thus the random coincidence events were effectively depressed by delimiting the energy and angle ranges of corresponding protons, as can be seen from Fig. 2(b)–(f) which display separately the coincidence ΔE–$E_{\rm r}$ scatter plots for the first to fifth rings of downstream MRSD. The ^{9}Li events for each ring were finally identified with the gate from Monte Carlo simulation, as shown in Fig. 2. The simulation took into account the kinematics, geometrical factor, angular- and energy-straggling effects in secondary target and ΔE detector, and has been calibrated with the ^{8}Li beam. About 50 ^{9}Li events were found for the $(CD_2)_n$ target runs, and no background event was found in the corresponding regions for the carbon target runs.

The differential cross section of ^{8}Li$(d, p)^9$Li can be expressed as

$$\frac{d\sigma}{d\Omega} = \frac{\Delta N}{I N_s \Delta\Omega \varepsilon}, \tag{1}$$

where ΔN, $\Delta\Omega$ and ε are respectively the number of $^9\mathrm{Li} - p$ coincidence events within the gate, the solid angle and coincidence efficiency of $^9\mathrm{Li} - p$ for each ring of downstream MRSD; I the number of incident ^{8}Li ions, and N_s the number of deuterium atoms per unit

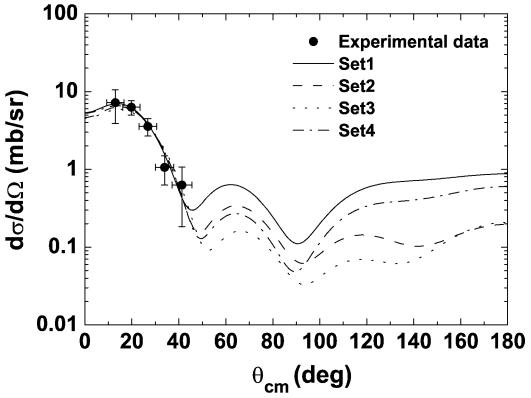

Fig. 3. Measured angular distribution of ^{8}Li$(d, p)^{9}$Li$_{\mathrm{g.s.}}$ at $E_{\mathrm{cm}} = 7.8$ MeV, together with DWBA calculations using different optical potential parameters.

area of $(CD_2)_n$ target. We performed a test experiment to verify the solid angle calculations for different rings of downstream MRSD using a ^{239}Pu source. This measurement yielded an isotropic angular distribution within the statistical uncertainties after normalized to the calculated solid angles, and thus demonstrated the correctness of calculation. Because of the existence of dead gaps in both MRSDs, a Monte Carlo simulation was carried out to ascertain the coincidence efficiency of $^{9}\mathrm{Li} - p$. This simulation also took the kinematics, geometric factor, angular- and energy-straggling effects into account. On the basis of the simulation, the coincidence efficiencies for different rings of downstream MRSD were deduced from the ratios of proton events in the relevant rings of upstream MRSD to ^{9}Li events in each ring of downstream one, ranging from 70 to 80%. The angular distribution in center of mass system for the ^{8}Li$(d, p)^{9}$Li (ground state) reaction was then obtained, as shown in Fig. 3. The uncertainty of differential cross section mainly resulted from the statistics and the assignment of ^{9}Li gate; the angular uncertainty arose from the angular divergence of ^{8}Li beam, the finite size of beam spot, the angular straggling in the target and ΔE detector as well as the width of each ring of the downstream MRSD.

The spins and parities of ^{8}Li and ^{9}Li (ground state) are 2^{+} and $3/2^{-}$, respectively. The ^{8}Li$(d, p)^{9}$Li$_{\mathrm{g.s.}}$ cross section includes two contributions from the neutron transfers to $1p3/2$ and $1p1/2$ orbits in ^{9}Li. If the reaction is dominated by peripheral process, the differential cross section can be expressed as

$$\left(\frac{d\sigma}{d\Omega}\right)_{\mathrm{exp}} = \frac{C_d^2}{b_d^2}\left[\left(C_{1,3/2}^{^{9}\mathrm{Li}}\right)^2 \frac{\sigma_{1,3/2}(\theta)}{(b_{1,3/2}^{^{9}\mathrm{Li}})^2} + \left(C_{1,1/2}^{^{9}\mathrm{Li}}\right)^2 \frac{\sigma_{1,1/2}(\theta)}{(b_{1,1/2}^{^{9}\mathrm{Li}})^2}\right], \tag{2}$$

where $(\frac{d\sigma}{d\Omega})_{\mathrm{exp}}$ and $\sigma_{l,j}(\theta)$ denote the measured and DWBA differential cross sections, respectively. C_d is the ANC for the virtual decay $d \to p + n$, $C_{1,3/2}^{^{9}\mathrm{Li}}$ and $C_{1,1/2}^{^{9}\mathrm{Li}}$ are ANCs for the virtual decay $^{9}\mathrm{Li} \to {}^{8}\mathrm{Li} + n$, corresponding to the $j = 3/2$ and $1/2$ orbits, $b_{l,j}^{^{9}\mathrm{Li}}$ and b_d being the single particle ANCs of the bound state neutrons in ^{9}Li and d. C^2/b^2 is so-called spectroscopic factor $S_{l,j}$.

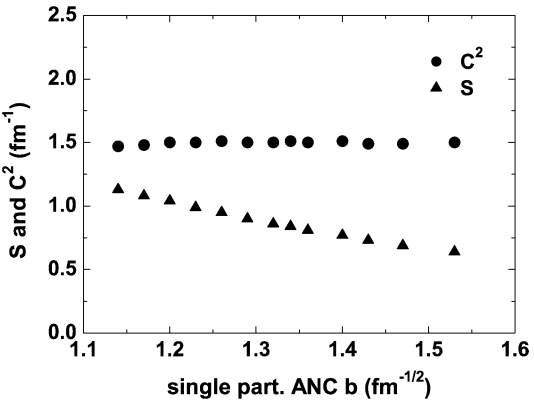

Fig. 4. Variation of the spectroscopic factor S and the square of ANC C^2 for $^9\mathrm{Li} \to {}^8\mathrm{Li} + n$ as functions of the single particle ANC b.

Table 1
Optical potential parameters used in DWBA calculations and the corresponding ANCs, where V, W are in MeV, r and a are in fm, the geometrical parameter of single particle bound state was set to be $r_0 = 1.25$ fm and $a = 0.65$ fm

Set No.	1		2		3		4	
Channel	Entrance	Exit	Entrance	Exit	Entrance	Exit	Entrance	Exit
V_r	142.9	41.9	118.0	41.9	118.0	66.37	142.9	66.37
r_{0r}	0.908	1.38	1.00	1.38	1.00	1.14	0.908	1.14
a_r	0.88	0.65	0.94	0.65	0.94	0.57	0.88	0.57
W_s	3.7	10.2	6.87	10.2	6.87	6.85	3.7	6.85
r_{0s}	2.26	1.5	1.98	1.5	1.98	1.14	2.26	1.14
a_s	0.67	0.37	0.59	0.37	0.59	0.5	0.67	0.5
V_{SO}	5.7	4.5	8.5	4.5	8.5	5.5	5.7	5.5
$r_{0\mathrm{SO}}$	0.908	1.35	1.00	1.35	1.00	1.14	0.908	1.14
a_{SO}	0.88	0.33	0.94	0.33	0.94	0.57	0.88	0.57
r_{0c}	1.38	1.33	1.30	1.33	1.30	1.14	1.38	1.14
$(C^{^9\mathrm{C}}_{1,3/2})^2$	1.68 ± 0.23		1.33 ± 0.19		1.27 ± 0.19		1.02 ± 0.16	

The finite-range distorted wave Born approximation (DWBA) code PTOLEMY [16] was utilized to compute the angular distributions. All optical potential parameters of the entrance channel were taken from Ref. [17], those of the exit channel from Refs. [17,18], respectively. The spectroscopic factors and the ANCs for $^9\mathrm{Li} \to {}^8\mathrm{Li} + n$ were computed by changing the radius r_0 and diffuseness a of Woods–Saxon potential for single particle bound state using one set of the optical potential parameters, as shown in Fig. 4. One can see that the spectroscopic factors vary strikingly, while the ANCs are nearly a constant, indicating that the $^8\mathrm{Li}(d, p)^9\mathrm{Li}_{\mathrm{g.s.}}$ reaction at present energy is dominated by peripheral process. In DWBA calculations, C_d was taken as 0.872 $\mathrm{fm}^{-1/2}$ from Ref. [19], and only the neutron transfer to the $1p3/2$ orbit was taken into account because the contribution of the $1p1/2$ orbit is less than 5% [4,5]. Fig. 3 presents the normalized angular distributions for four sets of optical potential parameters listed in Table 1. For each set, five $(C^{^9\mathrm{Li}}_{1,3/2})^2$ values

with different statistical errors were derived by fitting experimental points, the weighted average value of them was taken as the square of ANC value. The mean value of the four weighted average $(C^{^9\mathrm{Li}}_{1,3/2})^2$ values was 1.33 ± 0.33 fm^{-1}, the uncertainty arose from the error transfer of four ANCs (15%) and their deviation (20%).

3. Theoretical analysis of the $^8\mathrm{B}(p,\gamma)^9\mathrm{C}$ reaction

Very recently, the relationship of the ANCs for the mirror systems has been established [20,21]. The ground states of ^{9}C and ^{9}Li are mirror nuclei, the ANC for $^9\mathrm{C} \to {}^8\mathrm{B} + p$ can be related to that for $^9\mathrm{Li} \to {}^8\mathrm{Li} + n$ via

$$\left(C^{^9\mathrm{C}}_{1,3/2}\right)^2 = \left|\frac{F_l(ik_pR_N)}{k_pR_N j_l(ik_nR_N)}\right|^2 \left(C^{^9\mathrm{Li}}_{1,3/2}\right)^2, \tag{3}$$

where F_l and j_l are the regular Coulomb wave function and the Bessel function, respectively. k_p and k_n are the wave numbers of proton and neutron determined with their separation energies. The ratio of $(C^{^9\mathrm{C}}_{1,3/2})^2/(C^{^9\mathrm{Li}}_{1,3/2})^2$, $\left|\frac{F_l(ik_pR_N)}{k_pR_N j_l(ik_nR_N)}\right|^2$, is nearly a constant (around 0.89) when R_N changes from 2.5 to 5.0 fm in the calculations.

On the other hand, if we assume that the spectroscopic factors S_p and S_n are equal for mirror pairs, based on the relationship of spectroscopic factor and ANC, $C_{p(n)} = \sqrt{S_{p(n)}} \times b_{p(n)}$, the ANC for $^9\mathrm{C} \to {}^8\mathrm{B} + p$ can also be derived with

$$\left(C^{^9\mathrm{C}}_{1,3/2}\right)^2 = \left(C^{^9\mathrm{Li}}_{1,3/2}\right)^2 \left(b^{^9\mathrm{C}}_{1,3/2}\right)^2 / \left(b^{^9\mathrm{Li}}_{1,3/2}\right)^2. \tag{4}$$

The ratio of the proton and neutron single particle (ANCs)^2 for ^{9}C and ^{9}Li was extracted to be $(b^{^9\mathrm{C}}_{1,3/2})^2/(b^{^9\mathrm{Li}}_{1,3/2})^2 = 0.83$ from the single particle wave functions calculated with optical potential models. It should be noted that, in the calculations of the single particle wave functions, one must use the same r_0 and a, the same spin–orbit interaction for Woods–Saxon potentials, and the depths are adjusted to reproduce the neutron and proton binding energies of ^{9}Li and ^{9}C, respectively.

Combining the results from above two calculations, $(C^{^9\mathrm{C}}_{1,3/2})^2$ was derived to be 1.14 ± 0.29 fm^{-1} by Eq. (3) and Eq. (4). The error was mainly caused by the uncertainty of $(C^{^9\mathrm{Li}}_{1,3/2})^2$ as well as the systematic deviation of two ANC ratios (0.89 and 0.83).

At the temperatures of astrophysical interest, the direct capture of $^8\mathrm{B}(p,\gamma)^9\mathrm{C}$ reaction is believed to be dominated by the E1 transition from incoming s waves to bound p states. The direct capture amplitude for E1 transitions is given by

$$T_{1m} = \left\langle I^{^9\mathrm{C}}_{^8\mathrm{B}p}(\vec{r}) \middle| e_{\mathrm{eff}} r Y_{1m}(\Omega) \middle| \Psi^{(+)}_{\vec{k}}(\vec{r}) \right\rangle, \tag{5}$$

where $e_{\mathrm{eff}} = eN/A$ is the E1 effective charge for protons, N and A are the neutron and mass numbers of the whole system, respectively. $\Psi^{(+)}_{\vec{k}}(\vec{r})$ refers to the scattering wave function in the initial state, describing the relative motion between proton and ^{8}B. The overlap integral of the bound state wave functions for ^{8}B, proton and ^{9}C is

$$I^{^9\mathrm{C}}_{^8\mathrm{B}p}(\vec{r}) = \left\langle \phi_p(\xi_p)\phi_{^8\mathrm{B}}(\xi_{^8\mathrm{B}}) \middle| \phi_{^9\mathrm{C}}(\xi_p, \xi_{^8\mathrm{B}}, \vec{r}) \right\rangle, \tag{6}$$

where $\vec{r}$ is distance vector between proton and ^{8}B, and ξ_s the intrinsic coordinates for the particles labeled by their subscripts. The radial part of the overlap integral, $I_{l_f j_f}(r)$, from the multipole expansion of $I^{^9\mathrm{C}}_{^8\mathrm{B}p}(\vec{r})$, depends on the relative orbit angular momentum l_f of the captured proton to the ^{8}B core in the bound state j_f of ^{9}C. At very low energies of astrophysical relevance, the capture reaction is almost peripheral and thus the radial overlap function has the asymptotic behavior

$$I_{l_f j_f}(r) = C_{l_f j_f} W(2k_B r)/r, \quad r \geqslant R_N, \tag{7}$$

where $C_{l_f j_f}$ stands for ANC of $^9\mathrm{C} \to {}^8\mathrm{B} + p$. R_N denotes the nuclear interaction radius of proton and ^{8}B, which was empirically taken as $R_N = 1.3(A^{1/3} + 1)$ fm $= 4.0$ fm in the present calculation. $W(2k_B r)$ represents the Whittaker function, k_B the wave number for the bound state.

For s-wave incoming protons, the cross section for E1 capture to the ground state of ^{9}C can be calculated by

$$\sigma = \frac{16\pi}{9}\left(\frac{E_\gamma}{\hbar c}\right)^3 \frac{1}{\hbar v}\frac{e^2_{\mathrm{eff}}}{k^2}\frac{(2J_f+1)}{(2I_1+1)(2I_2+1)}\left(C^{^9\mathrm{C}}_{1,3/2}\right)^2 \times \left|\int_{R_N}^{\infty} r\,dr\, f_{lj}(kr) W(2k_B r)\right|^2, \tag{8}$$

where E_γ, v, I_1 and I_2 are the γ-ray energy, relative velocity between proton and ^{8}B, spins of proton and ^{8}B, respectively. $f_{lj}(kr)$ is the distorted radial wave function for the entrance channel, which can be calculated with DWBA, $k = \sqrt{2\mu E_{\mathrm{cm}}}/\hbar$ stands for the incident wave number. Since there exists Coulomb barrier, the cross section of peripheral proton capture is not sensitive to the optical potential parameters. We have checked the sensitivity of S-factors to the optical potentials, the uncertainty was less than 3% for $E_{\mathrm{cm}} \leqslant 0.6$ MeV. Thus, the direct capture $^8\mathrm{B}(p,\gamma)^9\mathrm{C}$ cross section only depends on the ANC, $(C^{^9\mathrm{C}}_{1,3/2})^2$.

The energy dependence of astrophysical S-factors for the direct capture of $^8\mathrm{B}(p,\gamma)^9\mathrm{C}$ reaction is shown in Fig. 5. The astrophysical $S_{18}(0)$ factor was found to be 44 ± 11 eV b. Fig. 6 shows the astrophysical $S_{18}(0)$ factors extracted from theoretical calculations and experiments. Our result is in good agreement with those in Refs. [5,6,8], but significantly smaller than that reported in Ref. [7]. The weighted average value of five experimental results was 48 ± 3 eV b, as indicated by two dashed lines in Fig. 6.

The reaction rate for the direct capture ($\mathrm{cm}^3\,\mathrm{mol}^{-1}\,\mathrm{s}^{-1}$) can be computed by [22],

$$N_A\langle\sigma v\rangle = 3.7313 \times 10^{10}\mu^{-1/2}T_9^{-3/2}\int_0^{\infty}\sigma E \exp(-11.605E/T_9)\,dE, \tag{9}$$

where μ is the reduced mass in amu, T_9 is the temperature in unit of 10^9 K, σ and E are cross section in barn and the center of mass energy in MeV, respectively. We have also calculated the contribution from a single level resonance ($E_x = 2.218$ MeV) with the Breit–Wigner formula. In this calculation, the partial widths were taken as $\Gamma_p \approx \Gamma = 100 \pm 20$ keV [23] and $\Gamma_\gamma = 34$ meV [1], respectively. The temperature dependence of the

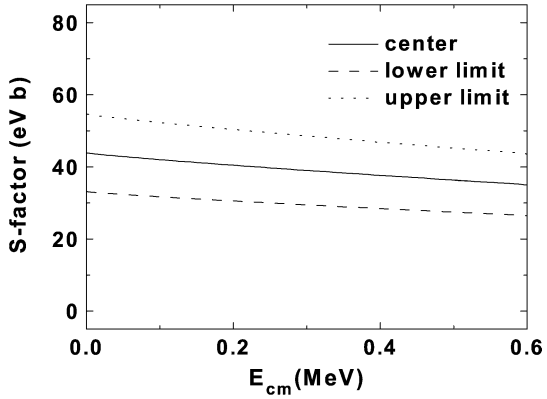

Fig. 5. Astrophysical S-factors as a function of $E_{\rm cm}$ for the direct capture $^8\mathrm{B}(p,\gamma)^9\mathrm{C}$ reaction.

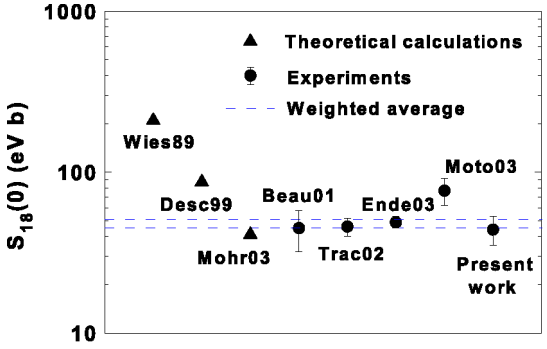

Fig. 6. Astrophysical $S_{18}(0)$ factors extracted from theoretical calculations and experiments.

$^8\mathrm{B}(p,\gamma)^9\mathrm{C}$ direct and resonant capture rates from present work is shown in Fig. 7. It can be seen that the direct capture dominates the $^8\mathrm{B}(p,\gamma)^9\mathrm{C}$ reaction in the temperature range of astrophysical interest and will thus determine the depletion of $^8\mathrm{B}$ in competition with the β-decay.

4. Summary and conclusion

Determination of reaction cross section on short-lived nuclear species is a major challenge for nuclear physics and nuclear astrophysics. Many of these reactions are difficult to measure directly with currently available experimental techniques because these species are too short-lived to serve as targets and the intensities of their ion beams are very low. It is therefore important to explore alternative methods for determining reaction cross sections on unstable nuclei. The ANC approach has been successfully applied to peripheral capture reactions in recent years. We utilized the peripheral neutron transfer reaction $^8\mathrm{Li}(d,p)^9\mathrm{Li}_{\mathrm{g.s.}}$ to deduce the ANC for the virtual decay $^9\mathrm{Li}\rightarrow{}^8\mathrm{Li}+n$ based on DWBA analysis for the first time. The ANC for $^9\mathrm{C}\rightarrow{}^8\mathrm{B}+p$ was then extracted by using charge

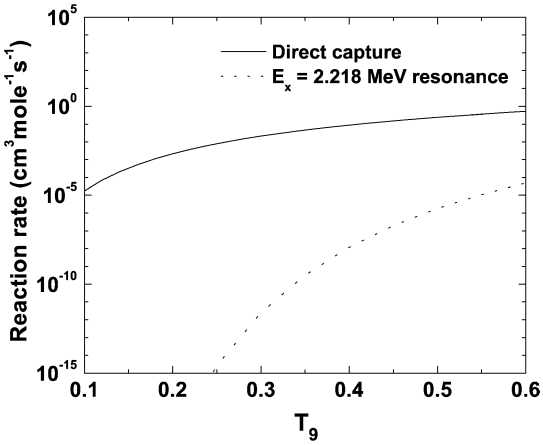

Fig. 7. Temperature dependence of the ^{8}B$(p,\gamma)^9$C reaction rates.

symmetry. In addition, we have calculated the direct capture S-factors and reaction rates for ^{8}B$(p,\gamma)^9$C at energies of astrophysical interest. Our work provides an independent examination to the existing results for the ^{8}B$(p,\gamma)^9$C reaction.

Acknowledgements

The authors would like to thank Dr. Natalia Timofeyuk for her help on the theoretical calculations of $(C^{^9\mathrm{C}}_{1,3/2})^2/(C^{^9\mathrm{Li}}_{1,3/2})^2$. This work was performed with the support of the Major State Basic Research Development Program under Grant Nos. G200077400 and 2003CB716704, the National Natural Science Foundation of China under Grant Nos. 10375096 and 10025524.

References

[1] M. Wiescher, J. Görres, S. Graff, L. Buchmann, F.-K. Thielemann, Astrophys. J. 343 (1989) 352.
[2] G.M. Fuller, S.E. Woosley, T.A. Weaver, Astrophys. J. 307 (1986) 675.
[3] P. Descouvemont, Nucl. Phys. A 646 (1999) 261.
[4] P. Mohr, Phys. Rev. C 67 (2003) 065802.
[5] D. Beaumel, T. Kubo, T. Teranishi, H. Sakurai, S. Fortier, A. Mengoni, N. Aoi, N. Fukuda, M. Hirai, N. Imai, H. Iwasaki, H. Kumagai, H. Laurent, S.M. Lukyanov, J.M. Maison, T. Motobayashi, T. Nakamura, H. Ohnuma, S. Pita, K. Yoneda, M. Ishihara, Phys. Lett. B 514 (2001) 226.
[6] L. Trache, F. Carstoiu, A.M. Mukhamedzhanov, R.E. Tribble, Phys. Rev. C 66 (2002) 035801.
[7] T. Motobayashi, Nucl. Phys. A 719 (2003) 65c.
[8] J. Enders, T. Baumann, B.A. Brown, N.H. Frank, P.G. Hansen, P.R. Heckman, B.M. Sherrill, A. Stolz, M. Thoennessen, J.A. Tostevin, E.J. Tryggestad, S. Typel, M.S. Wallace, Phys. Rev. C 67 (2003) 064301.
[9] B. Blank, C. Marchand, M.S. Pravikoff, T. Baumann, F. Boué, H. Geissel, M. Hellström, N. Iwasa, W. Schwab, K. Sümmerer, M. Gai, Nucl. Phys. A 624 (1997) 242.
[10] R.J. Glauber, in: W.E. Brittin, L.G. Dunham (Eds.), Lectures in Theoretical Physics, Interscience, New York, 1959.

[11] M.J. Balbes, M.M. Farrell, R.N. Boyd, X. Gu, M. Hencheck, J.D. Kalen, C.A. Mitchell, J.J. Kolata, K. Lamkin, R. Smith, R. Tighe, K. Ashktorab, F.D. Becchetti, J. Brown, D. Roberts, T.-F. Wang, D. Humphrey, G. Vourvopoulos, M.S. Islam, Nucl. Phys. A 584 (1995) 315.
[12] A.H. Wuosmaa, K.E. Rehm, J.P. Greene, D.J. Henderson, R.V.F. Janssens, C.L. Jiang, L. Jisonna, E.F. Moore, R.C. Pardo, M. Paul, D. Peterson, S.C. Pieper, G. Savard, J.P. Schiffer, R.E. Segel, S. Sinha, X. Tang, R.B. Wiringa, Phys. Rev. Lett. 94 (2005) 082502.
[13] Z.H. Li, W.P. Liu, X.X. Bai, B. Guo, G. Lian, S.Q. Yan, B.X. Wang, S. Zeng, Y. Lu, J. Su, Y.S. Chen, K.S. Wu, N.C. Shu, T. Kajino, Phys. Rev. C 71 (2005) 052801(R).
[14] X. Bai, W. Liu, J. Qin, Z. Li, S. Zhou, A. Li, Y. Wang, Y. Cheng, W. Zhao, Nucl. Phys. A 588 (1995) 273c.
[15] W. Liu, Z. Li, X. Bai, Y. Wang, G. Lian, S. Zeng, S. Yan, B. Wang, Z. Zhao, T. Zhang, H. Tang, B. Yang, X. Guan, B. Cui, Nucl. Instrum. Methods Phys. Res. B 204 (2003) 62.
[16] M. Rhoades-Brown, M.H. Macfarlane, S.C. Pieper, Phys. Rev. C 21 (1980) 2417;
M. Rhoades-Brown, M.H. Macfarlane, S.C. Pieper, Phys. Rev. C 21 (1980) 2436.
[17] C.M. Perey, F.G. Perey, At. Data Nucl. Data Tables 17 (1976) 1.
[18] B.A. Watson, P.P. Singh, R.E. Segel, Phys. Rev. 182 (1969) 977.
[19] L.D. Blokhintsev, I. Borbely, E.I. Dolinskii, Sov. J. Part. Nucl. 8 (1977) 485.
[20] L. Trache, A. Azhari, F. Carstoiu, H.L. Clark, C.A. Gagliardi, Y.-W. Lui, A.M. Mukhamedzhanov, X. Tang, N. Timofeyuk, R.E. Tribble, Phys. Rev. C 67 (2003) 062801(R).
[21] N.K. Timofeyuk, R.C. Johnson, A.M. Mukhamedzhanov, Phys. Rev. Lett. 91 (2003) 232501.
[22] C. Angulo, M. Arnould, M. Rayet, P. Descouvemont, D. Baye, C. Leclercq-Willain, A. Coc, S. Barhoumi, P. Aguer, C. Rolfs, R. Kunz, J.W. Hammer, A. Mayer, T. Paradellis, S. Kossionides, C. Chronidou, K. Spyrou, S. Degl'Innocenti, G. Fiorentini, B. Ricci, S. Zavatarelli, C. Providencia, H. Wolters, J. Soares, C. Grama, J. Rahighi, A. Shotter, M. Lamehi-Rachti, Nucl. Phys. A 656 (1999) 3.
[23] F. Ajzenberg-Selove, Nucl. Phys. A 413 (1984) 1.